Mechanics of Materials 157 (2021) 103818

Contents lists available at ScienceDirect

Mechanics of Materials

journal homepage: www.elsevier.com/locate/mechmat

Shear modulus of conventional and auxetic open-cell foam

Nejc Novak [a,*], Olly Duncan [b,c], Tom Allen [c], Andrew Alderson [b], Matej Vesenjak [a], Zoran Ren [a]

[a] Faculty of Mechanical Engineering, University of Maribor, Maribor, Slovenia
[b] Materials and Engineering Research Institute, Sheffield Hallam University, Sheffield, UK
[c] Department of Engineering, Manchester Metropolitan University, Manchester, UK

ARTICLE INFO

Keywords:
Shear modulus
Open-cell foam
Auxetic behaviour
Poisson's ratio
Young's modulus

ABSTRACT

This work analyses shear moduli of conventional and auxetic open-cell polymer foams. Shear moduli are i) measured directly and ii) calculated by applying elasticity theory for isotropic solid materials, using Young's moduli and Poisson's ratios from compression tests. Zero and negative Poisson's ratio foams are fabricated from conventional foams using a thermo-mechanical process. Fabricated and conventional foams are compression tested in three orthogonal directions, up to densification at ~60% compression, with full-field strain measurements obtained using Digital Image Correlation. Compression testing is followed by shear testing. The measured shear moduli vary from 16±7 kPa for negative Poisson's ratio foams to 38±2 kPa for zero Poisson's ratio foams, with conventional foams in between with a mean value of 32±8 kPa. The calculated shear moduli are typically lower than the measured values. The results suggest that the application of elasticity theory to calculate the low strain shear modulus of open-cell foam from Young's modulus and Poisson's ratio measured in compression tests is appropriate if the foam is isotropic.

1. Introduction

The shear modulus G of an elastic, isotropic bulk material depends on Young's modulus E and Poisson's ratio ν (Timoshenko and Goodier, 1970):

$$G = \frac{E}{2(1+\nu)} \tag{1}$$

According to Equation (1), shear modulus increases with Young's modulus, or as Poisson's ratio decreases. Indeed, Equation (1) indicates that shear modulus tends to infinity as Poisson's ratio tends to −1.

There has been little work applying Equation (1) to cellular foams. The shear moduli of foams with positive Poisson's ratios were calculated using analytical modelling (Zhu et al., 1997), and rheology for high compression levels (Andersson et al., 2008). A negative Poisson's ratio (NPR) close to −1 was inferred from Equation (1) over a limited strain range, from Young's and shear moduli, and supported by images of the foam showing re-entrant cellular structure during compression tests (Andersson et al., 2008). Andersson and colleagues did not actually measure Poisson's ratio and recognised that Equation (1) does not account for anisotropy, also seen in the microscopic images of the foam. As such, the use of Equation (1) to calculate Poisson's ratio from the Young's and shear moduli of the foam may have been erroneous (Andersson et al., 2008).

Materials exhibiting NPR are called auxetic materials (Evans et al., 1991; Kelkar et al., 2020; Kolken and Zadpoor, 2017; Lurie et al., 2018). Auxetic materials expand laterally under tension and shrink laterally under compression, and can include foams (Chan and Evans, 1997; Lakes, 1987), honeycombs (Brighenti et al., 2016) and additively manufactured structures (Li et al., 2017; Shepherd et al., 2020). Auxetic open-cell foam is typically thermo-mechanically fabricated by heating and then cooling conventional foam while imposing volumetric compression (Chan and Evans, 1997; Lakes, 1987), although softening agents such as carbon dioxide (Li and Zeng, 2016) or solvents (Grima et al., 2009) can substitute for heat. The magnitude of NPR achieved with thermo-mechanical fabrications depends on both the applied volumetric compression and heat exposure (Duncan et al., 2019). By applying a high temperature or long heating time in the processing window for a thermo-mechanical fabrication, it is possible to make foams with a Poisson's ratio close to zero (Chan and Evans, 1998; Duncan et al., 2019), herein referred to as ZPR. Studies on indentation testing of auxetic open-cell foams have varied heating conditions and volumetric compression to make samples with a range of Poisson's ratios, but of similar size and density (Chan and Evans, 1998).

* Corresponding author.
E-mail address: n.novak@um.si (N. Novak).

https://doi.org/10.1016/j.mechmat.2021.103818
Received 19 October 2020; Received in revised form 22 February 2021; Accepted 28 February 2021
Available online 12 March 2021

Studies have compared analytical and finite element model predictions to experimental test results for auxetic cellular structures (Jin et al., 2019; Lira et al., 2009). How cellular structure influences the shear modulus of auxetic foams has also been reported (Cheng et al., 2018). This work compares shear modulus obtained by experimental measurement and calculation according to Equation (1), for auxetic and conventional open-cell foam. The work examines the validity of estimating shear modulus using compression testing and digital image correlation (DIC), without the need for shear testing. Samples are typically fixed to the test rig during shear testing (Novak et al., 2020), meaning they become damaged and cannot be reused, such as for testing in other orientations.

2. Experimental methods

2.1. Geometry and fabrication of samples

Two sets of foam samples were fabricated based on previous work with the same open-cell polyurethane (PU) foam (PUR30 FR, supplied by Custom Foams) (Duncan et al., 2019). Foam cuboids (32 × 32 × 96 mm) were compressed into aluminium moulds with isotropic volumetric compression ratios (VCRs, original/final volume) of three or five, then heated in an oven for 20 min at 180 or 160 °C, respectively. These conditions were selected to give foams with a range of Poisson's ratio and stiffness. Unconverted foam samples were cut with a utility knife (Stanley) to similar size as the fabricated samples, for comparative testing. Direction 1 (Fig. 1) corresponds to the cell rise direction (Gibson and Ashby, 1997), which was positioned across the mould (parallel to the 32 mm dimension) and is illustrated in Fig. 1 with a hexagon.

2.2. Compression and shear testing

Quasi-static compression (Fig. 2a) and shear tests (Fig. 2b) were carried out using a Tinius Olsen H10KT testing machine. Compression plates (compression testing) and a flat-faced rig (shear testing) with a 250 N load cell were used, following an ISO standard (*ISO, 20114:2011 - Mechanical testing of metals - ductility testing - compression test for porous and cellular metals*, 2011). A preload of 0.5 N was applied to ensure contact between the sample and compression plates. The loading rate was 50 mm/min, resulting in strain rates between 0.017 s^{-1} and 0.024 s^{-1}, depending on the size of the sample. Samples were compressed to ~60% engineering strain in each loading direction and left to recover for about an hour before retesting in a different orientation.

The shear-loading device consisted of two stiff parallel plates, attached to the samples with epoxy resin, Fig. 2b. The parallel plates were much stiffer than the foam and were not seen to bend nor deflect during testing. Eight unconverted (UC), six ZPR and nine NPR samples were tested, Table 1. UC and NPR samples were tested to failure in each of the three orthogonal directions, while ZPR samples were tested only in two orthogonal directions (direction 1 and 2). As the linear displacement of the shear plates increased, the device imparted both shear deformation and axial tension. Almost pure shear with negligible tension ($\leq$ 0.1%) was achieved until the linear displacement of the shear plates reached 5% of sample size (i.e. less than 5% applied shear strain). Tension began to increase rapidly after 5% shear strain (Fig. 2c), as calculated from the displayed equations concerning the original sample dimension and plate displacement. As such, pure shear could not be assumed above 5% applied shear strain (Fig. 2c).

2.3. Full-field strain measurement

Two-dimensional DIC (GOM Correlate, 2019)[1] was applied to measure incremental transverse and axial strains during compression tests, which were used to obtain Poisson's ratio (Allen et al., 2017; Duncan et al., 2019; Phillips et al., 2018). Images for DIC were captured with an HD SONY HDR-SR8 video camera (2848 × 2136 resolution, 25 Hz). A surface component (shown on Fig. 3a–c) with facet sizes of ~25 px, matching against the previous stage and "*More Points*" options selected, was defined across the central third of each sample (Fig. 2a). Mean incremental strains were calculated across the surface component, which did not include regions close to the compression plates, to avoid contact and boundary effects.

2.4. Analysis

Poisson's ratio, Young's modulus and shear modulus were obtained for all samples in each orientation. These elastic constants were obtained from the gradient of a straight line fitted over the initial linear elastic region of the lateral strain vs axial strain data (Poisson's ratio, corresponding to negative of gradient), stress vs strain data (Young's modulus) and shear stress vs shear strain data (shear modulus), corresponding to 0–2.5% compression or 0–1% shear strain. Mean and standard deviation (S.D.) values were calculated for a set of samples for each orientation. Coefficients of variation (S.D./Mean) in each orientation were below 20%. Pooled standard deviations between orientations were calculated from standard deviations in each tested orientation, according to (Stelman, (2018)):

$$S.D. = \sqrt{S.D._1^2 + S.D._2^2 + S.D._3^2} \quad (2)$$

A Bland – Altman plot (Bland and Altman, 2003) was used to compare the bias (mean difference) and limits of agreement (p = 0.95, 1.96 × standard deviations) between measured and calculated shear moduli for the three groups of samples.

3. Results of experimental testing

All experimental results are given as mean values. Specimen dimensions and masses are listed in Table 1. The UC foams were ~30% larger in all three directions and ~40% lighter than the ZPR and NPR foams, Table 1.

3.1. Compression testing

DIC images of transverse strain (direction 3) on the surface of UC, ZPR and NPR foam at different levels of applied compression in direction 1 are shown in Fig. 3. The mean transverse vs axial strain relationships are shown in Fig. 4. The mean transverse strains were calculated at incrementally increasing axial strains of ~0.01%.

The transverse strain on the face of the UC foam increased at a relatively constant rate until about 5–10% compression, then remained almost constant to 30% compression (Fig. 3a). The ZPR foam (Fig. 3b) expanded transversely towards the edges of the face and contracted transversely towards the centre. The NPR foam sample (Fig. 3c) showed almost even transverse contraction, with some variation across the face at 30% compression. The UC foam exhibited positive Poisson's ratio transverse expansion (Fig. 4). The ZPR foam exhibited low transverse strain, due to its expanding edges and contracting centre (Figs. 3a and 4). The NPR foam exhibited quasi-linear NPR transverse contraction (Fig. 4).

The Poisson's ratio (i.e. relationship between the transverse and axial strain) of all foams was not constant at higher strain (above 3% in the case of loading in direction 1 and above 8% in the case of loading in direction 2 and 3, Fig. 4). The non-linearity in transverse vs axial strain relations at higher strain was most pronounced for the UC foam (Fig. 4). The strain dependency of Poisson's ratio at higher strains is noted in the literature for isotropic elastic materials (Beatty and Stalnaker, 1986), and also for conventional and auxetic foams (Duncan et al., 2021; Li et al., 2016).

[1] https://www.gom.com/3d-software/gom-correlate.html.

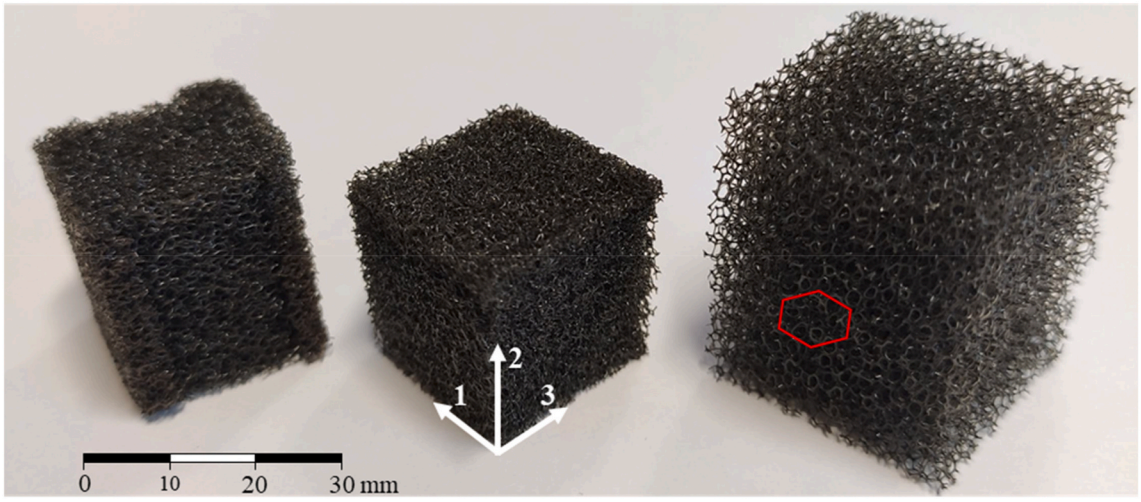

Fig. 1. Analysed samples (from left to right: NPR, ZPR and original unconverted foam). The red hexagon shows the elongated cell rise direction in the 1-2 plane (before conversion). The longest foam dimension in the mould was in direction 2. (For interpretation of the references to colour in this figure legend, the reader is referred to the Web version of this article.)

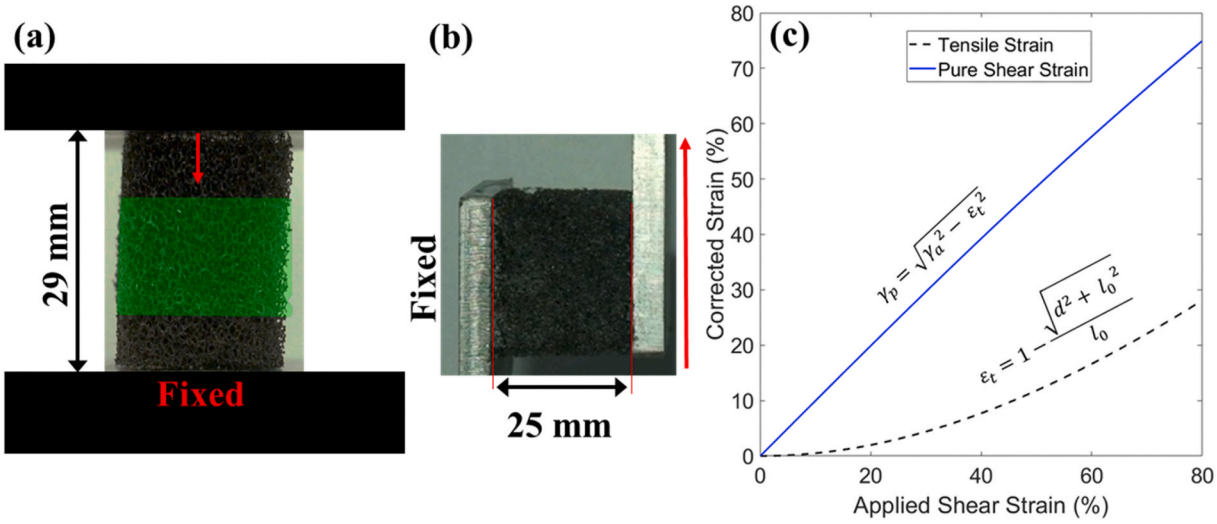

Fig. 2. a) Compression test set up, showing DIC surface component in green, b) shear test set up (red vertical arrow indicates the direction of loading, reference sample dimension labelled), c) tensile (ε_t) and pure shear (γ_p) strain vs applied (γ_a) strain, and equations used to calculate each from sample and device orientations and displacements (d is displacement, l_o is original width (e.g. 25 mm in (b)). Displayed sample in (a) and (b) is UC foam. (For interpretation of the references to colour in this figure legend, the reader is referred to the Web version of this article.)

Table 1
Dimensions, volume, mass and density of samples.

Specimen	Sample Nr.	Mean length (S.D.) [mm]			Volume [cm^3]	Mass [g]	Density [kg/m^3]
		Dir. 1	Dir. 2	Dir. 3			
UC	8	29 (0.4)	26 (0.5)	27 (0.9)	21	0.6 (0.03)	28
ZPR	6	22 (0.6)	21 (0.5)	21 (0.3)	10	1.0 (0.13)	98
NPR	9	23 (1.7)	21 (0.8)	21 (0.6)	10	1.0 (0.05)	97

Mean compressive stress vs strain relationships of all tests for UC, ZPR and NPR foams are shown in Fig. 5. Mean engineering stress was calculated at incrementally increasing axial strain of ~0.05%. The UC foam had the typical stress vs strain response (Fig. 5a) of hexagonal honeycomb-like cellular materials in loading direction 1 (aligned with the cell rise direction); a quasi-linear region until 3% strain, then a transition zone followed by a compressive stress plateau after ~5% strain (Gibson and Ashby, 1997). The plateau region started later in the other two directions, at about 8% strain (Fig. 5a). The stress vs strain responses in directions 2 and 3 were similar to each other, while direction 1 had a steeper gradient at low strains; consistent with the elongated cell rise typical of open-cell foam (Duncan et al., 2017; Gibson and Ashby, 1997; Lakes, 1987). The ZPR and NPR foam (Fig. 5b and c) had quasi-linear stress vs strain relationships. These stress vs strain relationships were almost isotropic for the ZPR foam (Fig. 5b), whereas for the NPR foam the gradient was steeper in direction 1 than in directions 2

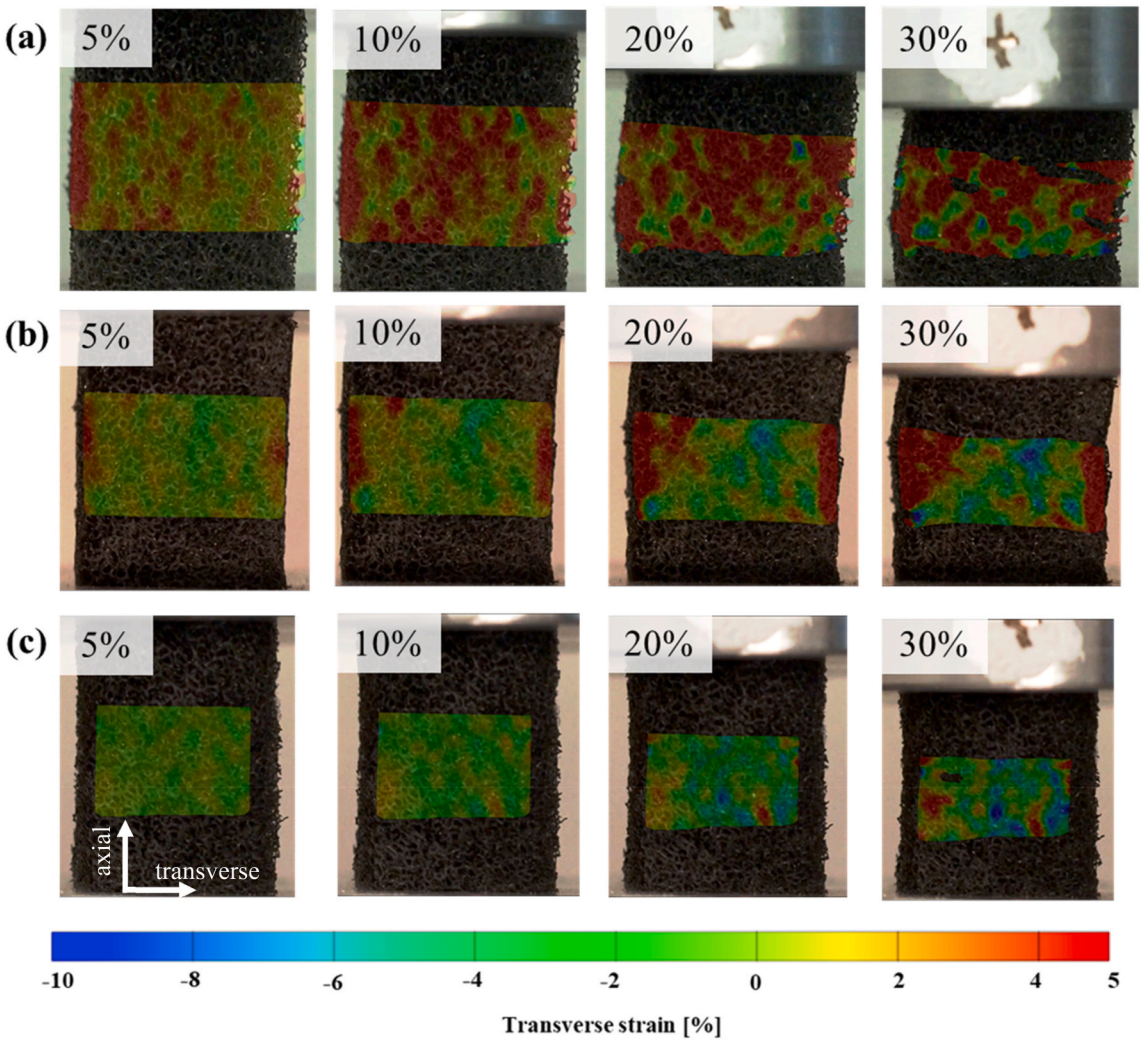

Fig. 3. DIC countour plots of transverse strain (direction 3) for UC foam (a), ZPR foam (b) and NPR foam (c) at 5%, 10%, 20% and 30% applied compression in direction 1.

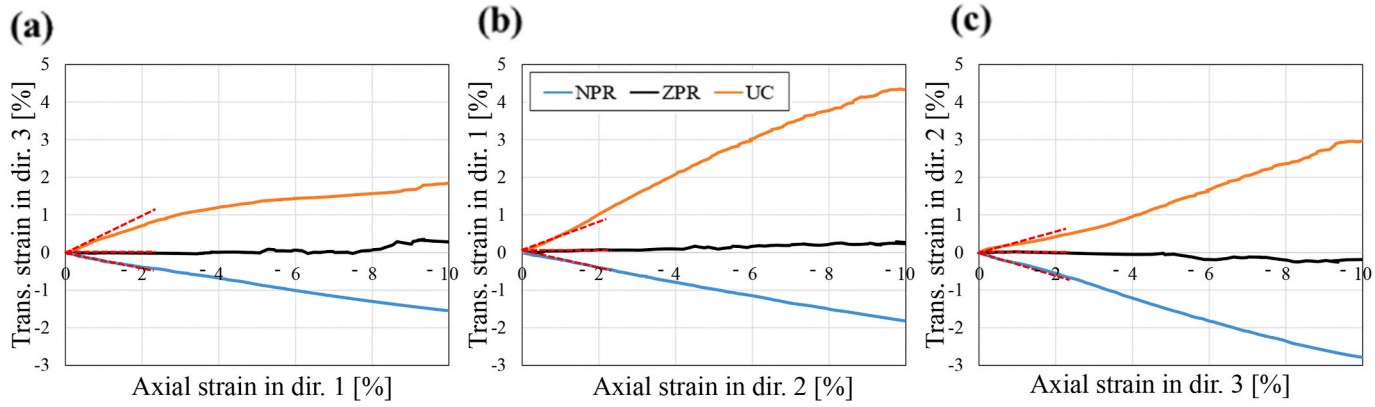

Fig. 4. Mean transverse vs axial strain plots for loading in direction 1 (a), direction 2 (b) and direction 3 (c). The linear trend lines (dashed red lines) represent the method used to obtain the initial, low strain Poisson's ratio. Legend in (b) applies to (a) and (c). (For interpretation of the references to colour in this figure legend, the reader is referred to the Web version of this article.)

and 3.

The measured Poisson's ratio and Young's modulus values (mean and S.D. across all samples) for all orientations and mean values (and S.D., Equation (2)) up to 2.5% compression are shown in Tables 2 and 3, respectively. Poisson's ratio values are written as ν_{ij}, where i denotes the loading direction and j denotes the transverse strain direction.

The compressive Poisson's ratios were almost isotropic for the ZPR and NPR foams, and orthotropic for the UC foam (Table 2). The Young's moduli of UC foams were similar in loading directions 2 and 3, and the Young's modulus was over twice these values in direction 1 (Table 3).

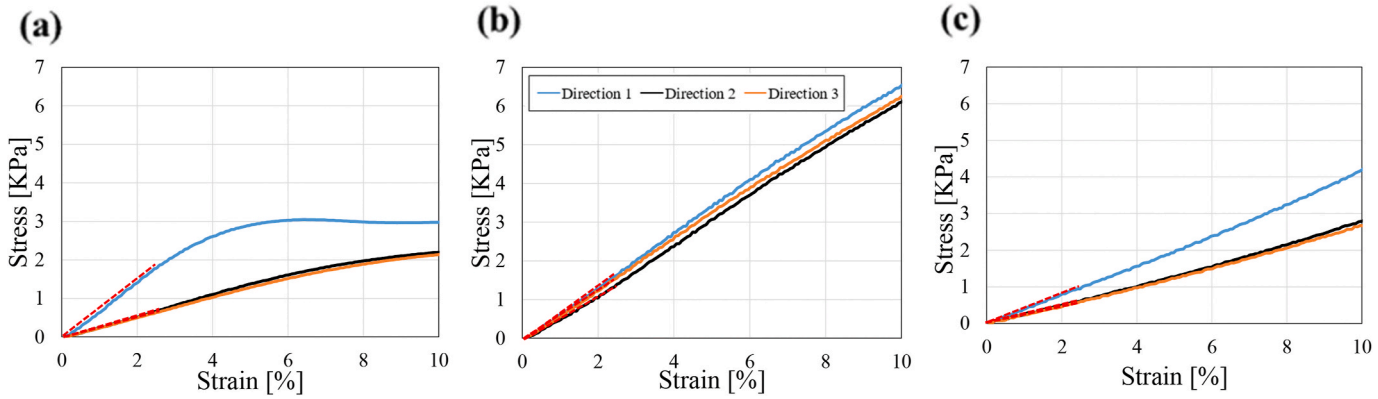

Fig. 5. Mean compressive stress vs strain relationships for UC (a), ZPR (b) and NPR (c) foams. The linear trend lines (dashed red lines) represent the region used to obtain a constant, low strain Young's modulus. Legend in (b) applies to (a) and (c). (For interpretation of the references to colour in this figure legend, the reader is referred to the Web version of this article.)

Table 2
Poisson's ratio values up to 2.5% compression (mean and S.D. across all samples), and the mean and S.D. (Equation (2)) Poisson's ratios for all orientations.

Specimen	ν_{13}	ν_{21}	ν_{32}	Mean ν
UC	0.6 (0.2)	0.3 (0.1)	0.3 (0.1)	0.4 (0.2)
ZPR	0.0 (0.1)	0.0 (0.1)	0.0 (0.1)	0.0 (0.1)
NPR	−0.2 (0.1)	−0.2 (0.1)	−0.3 (0.2)	−0.3 (0.2)

Table 3
Young's moduli up to 2.5% compression (mean and S.D. across all samples), and the mean and S.D. (Equation (2)) Young's moduli for all orientations.

Specimen	E_1 [kPa]	E_2 [kPa]	E_3 [kPa]	Mean [kPa]
UC	76 (17)	28 (4)	26 (5)	43 (18)
ZPR	50 (8)	58 (14)	66 (15)	58 (22)
NPR	40 (10)	25 (5)	24 (5)	30 (12)

The ZPR foam deformed almost isotropically. The NPR foams exhibited orthotropic behaviour, with Young's modulus in direction 1 almost twice the Young's moduli in directions 2 and 3.

3.2. Shear testing

Shear deformation of UC, ZPR and NPR foam samples is shown in Fig. 6. Pure shear was only achieved at small applied deformations (≤5% applied shear, causing ≤0.1% tension, Fig. 2c). As the applied deformation increased, the combination of shear, tension and a positive Poisson's ratio gave the UC foam a concave shape (Fig. 6a). The ZPR foams had a slightly convex shape during coupled shear and tensile loading (Fig. 6b), indicating NPR in tension. Slight expansion in tension was consistent with previous tests of similar ZPR foam, where tensile Poisson's ratios were slightly negative (0 to −0.1), and compressive values were close to zero (Duncan et al., 2019). The convex shape was clearest in the NPR foam samples (Fig. 6c).

Mean shear stress vs applied shear strain of UC, ZPR and NPR foam samples is shown in Fig. 7. Mean shear stress values were calculated at incrementally increasing axial shear strains of ~0.05%.

The shear stress vs strain relationships, and hence the shear moduli,

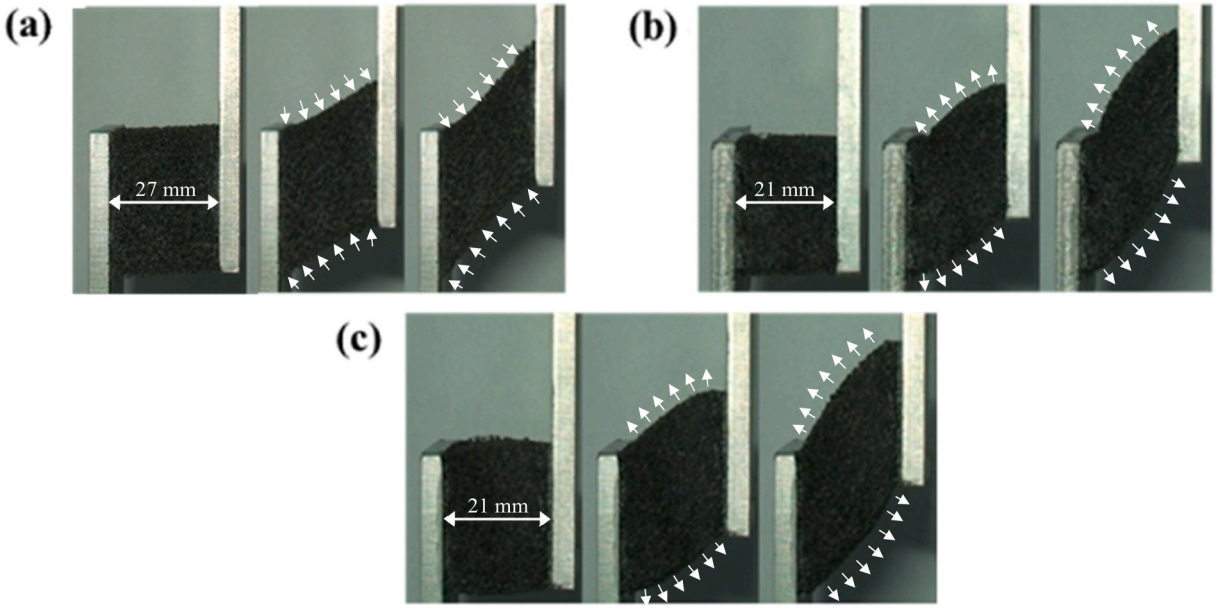

Fig. 6. Deformation of UC (a), ZPR (b) and NPR (c) foam samples under shear loading in direction 1, at 0%, ~40% and ~80% applied shear strain. Transverse dimensions were set to original sample widths (labelled) and maintained throughout the test.

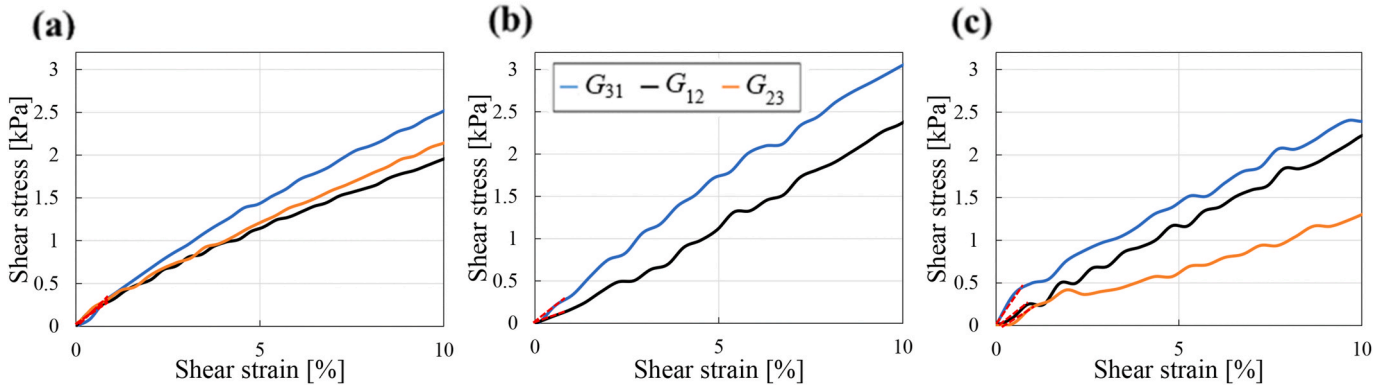

Fig. 7. Mean shear stress vs applied shear strain of UC (a), ZPR (b) and NPR (c) foam samples. The linear trend lines (dashed red lines) represent the region used to obtain an initial, low strain shear modulus. Legend in (b) applies to (a) and (c). (For interpretation of the references to colour in this figure legend, the reader is referred to the Web version of this article.)

of the UC foam were similar in all three loading directions (Fig. 7a). The shear stiffness of the ZPR foam in direction 1 (G_{31}) was higher (steeper gradient) than the shear stiffness in the direction 2 (G_{12}), Fig. 7b. For the NPR foam, the shear stress vs strain relationships in directions 1 and 2 (G_{31} and G_{12}) were similar, with lower stiffness (gradient) in direction 3 (G_{23}) at strains above 2% (Fig. 7c). The corresponding measured shear moduli for all foam samples (Table 4) were determined by fitting straight lines to shear stress vs strain relationships up to 1% applied shear (Fig. 7).

4. Comparison of calculated and measured shear moduli

In Table 4, the measured shear modulus G_m values were compared to calculated shear modulus G_c values from Equation (1), using Poisson's ratio (Table 2) and Young's modulus (Table 3). Shear modulus values are written as G_{ij}, where i denotes the transverse direction (i.e. between plates), and j denotes the loading direction (Fig. 2b).

The ZPR foams had the highest measured G_m and calculated G_c shear moduli (Table 4). The NPR foams had the lowest measured G_m values, whereas the lowest calculated G_c values were found for the UC foams. Differences between the measured and calculated values were observed, particularly for the orthotropic UC samples, although these decreased when a mean was taken between directions (Table 4).

The Bland-Altman plot shows that the mean measured shear modulus of UC samples was 13 kPa higher than when calculated from compression tests (Fig. 8). The mean measured shear moduli for both ZPR and NPR samples were 3 kPa higher than the calculated values. Despite the larger bias for the UC samples, the limits of agreement were narrower, between 3 and 23 kPa, than the −15 to 21 kPa and −13 to 19 kPa limits of agreement for the ZPR and NPR samples, respectively.

5. Discussion

Bias between measured and calculated shear moduli was highest for the orthotropic UC foam (13 ± 10 kPa). The more isotropic ZPR (3 ± 18 kPa) and NPR (3 ± 16 kPa) foams had less consistent but less bias values (Fig. 8). With elongated cell rise direction generally removed during thermo-mechanical conversions, which apply uniform compression (Chan and Evans, 1997; Duncan et al., 2019; Lakes, 1987), anisotropy in Poisson's ratio (Table 2), Young's modulus (Table 3) and shear modulus was reduced. Using a mean Poisson's ratio, Young's modulus and shear modulus across the three loading directions may have contributed to the differences observed in measured and calculated values for the UC foam (Fig. 8).

A broad range of Poisson's ratios (mean of −0.3 to 0.4, Table 2) and Young's moduli (mean of 30–58 kPa, Table 3) were obtained, as expected following similar thermo-mechanical conversions of open-cell foam (Chan and Evans, 1998; Duncan et al., 2019). As observed in previous work (Cheng et al., 2018), the low strain shear modulus (Table 4) of the UC foam (32 kPa, Table 4) was higher than for the NPR foam (23 kPa, Table 4), mainly due to the auxetic foam's lower Young's modulus (Fig. 5, Table 3). The shear moduli (10–38 kPa, Table 4) of the foams were lower than those reported previously (30–60 kPa (Cheng et al., 2018)) for higher strain rates (of 0.05–2.5 s^{-1}) than applied here (0.01–0.025 s^{-1}). The ZPR foam with higher Young's modulus had the highest mean measured shear modulus (33 kPa, Table 4).

Uncertainty in the measurement of foam shear modulus, with the coefficient of variation at almost 50% of measured values and 75% of calculated values (Table 4), hindered comparisons with calculated values. As such, this work highlights challenges in measuring and calculating the shear modulus of open-cell foam. Compression testing allowed each sample to be characterised in different orientations, but this was not possible with shear testing, where samples were glued to plates. High levels of applied shear (>5%) also imparted tension in the samples (Fig. 2c). For a better comparison of measured and calculated shear moduli over a wider strain range, further work could use a shear test rig capable of applying pure shear over a wider strain range. Such work could benefit from applying DIC to measure full-field strain during shear tests.

Table 4
Comparison of mean measured G_m and mean calculated G_c shear moduli (and S.D. for each sample and all orientations, with pooled S.D. calculated according to Equation (2)).

Specimen	G_{31}		G_{12}		G_{23}		Mean	
	G_m	G_c	G_m	G_c	G_m	G_c	G_m	G_c
UC	36	23	29	11	31	10	32	15
	(4)	(3)	(7)	(1)	(1)	(2)	(8)	(4)
ZPR	38	26	27	29	–	35	33	30
	(2)	(11)	(7)	(7)		(10)	(7)	(16)
NPR	27	26	25	15	16	17	23	20
	(5)	(12)	(6)	(3)	(7)	(7)	(11)	(15)

6. Conclusions

In this study, we analysed the shear moduli of conventional, zero Poisson's ratio and auxetic open-cell foams, obtained by experimental measurements and calculated from compressive Young's moduli and Poisson's ratios. The measured shear moduli varied between ~16 kPa for negative Poisson's ratio foams and 38 kPa for zero Poisson's ratio foams, with conventional foams in between at ~32 kPa. The mean values of measured shear moduli tended to be higher (23 kPa–33 kPa) than those calculated by applying elasticity theory (10–30 kPa). The measured and calculated values of shear modulus were compared using

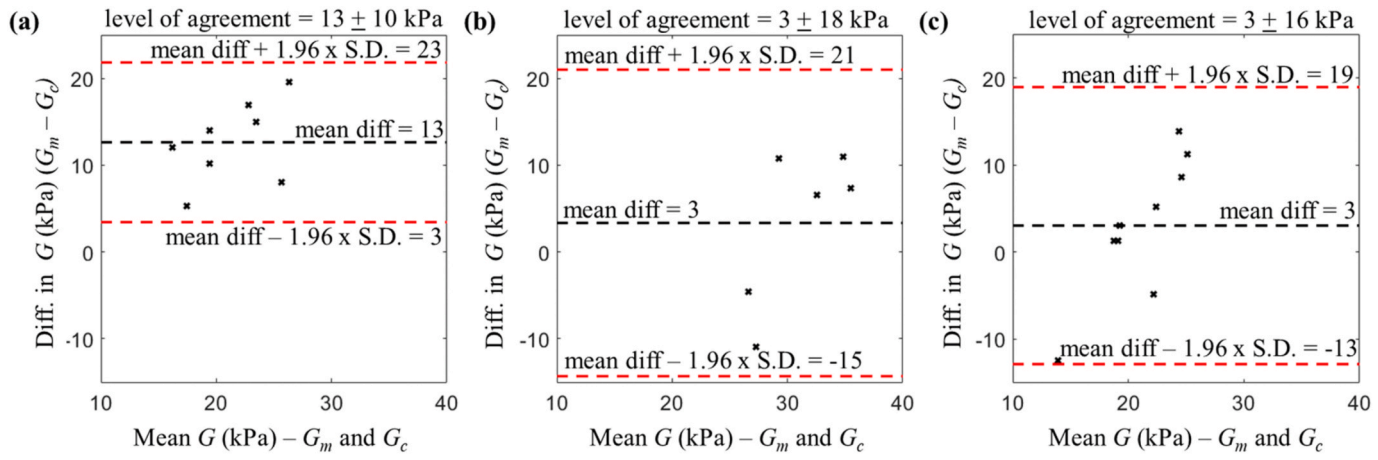

Fig. 8. Bland-Altman plot showing levels of agreement between measured shear moduli and those calculated by equation (1) for UC (a), ZPR (b) and NPR (c) samples.

Bland-Altman limits of agreement. The bias for the conventional foam was +13 kPa, with limits of agreement ($p = 0.95$) between 3 and 23 kPa. A bias of +3 kPa was obtained for both the zero and negative Poisson's ratio foam samples, with limits of agreement between −15 and 21 kPa and −13 and 19 kPa, respectively. These results suggest that using compression tests to calculate shear modulus, from Young's modulus and Poisson's ratio, is inappropriate for many conventional open-cell foams, which are anisotropic due to elongated cells in the rise direction. It is possible to estimate the shear modulus of isotropic auxetic foams from compression test data, as equal uniaxial compression applied during fabrication can remove anisotropy from cell rise direction.

Author statement

Nejc Novak: Conceptualization, Investigation, Writing – original draft. Olly Duncan: Conceptualization, Investigation, Validation, Writing – review & editing. Tom Allen: Investigation, Validation, Writing – review & editing. Andrew Alderson: Conceptualization, Funding acquisition, Supervision, Validation, Writing – review & editing. Matej Vesenjak: Conceptualization, Supervision, Validation, Writing – review & editing. Zoran Ren: Conceptualization, Funding acquisition, Supervision, Validation, Writing – review & editing

Declaration of competing interest

The authors declare no conflict of interest. The authors declare that they have no known competing financial interests or personal relationships that could have appeared to influence the work reported in this paper.

Acknowledgments

The research was performed within the framework of the basic postdoctoral research project (No. Z2-2648) and research core funding (No. P2-0063), financed by the Slovenian Research Agency. The support of the Erasmus + programme is also acknowledged.

References

Allen, T., Hewage, T., Newton-Mann, C., Wang, W., Duncan, O., Alderson, A., 2017. Fabrication of auxetic foam sheets for sports applications. Phys. Status Solidi Basic Res. 1700596, 1–6. https://doi.org/10.1002/pssb.201700596.

Andersson, A., Lundmark, S., Magnusson, A., Maurer, F.H.J., 2008. Shear behavior of flexible polyurethane foams under uniaxial compression. Polym. Polym. Compos. 111, 2290–2298.

Beatty, M.F., Stalnaker, D.O., 1986. The Poisson function of finite elasticity. J. Appl. Mech. 53, 807–813. https://doi.org/10.1115/1.3171862.

Bland, J.M., Altman, D.G., 2003. Applying the right statistics : analyses of measurement studies. Ultrasound Obstet. Gynecol. 22, 85–93. https://doi.org/10.1002/uog.122.

Brighenti, R., Spagnoli, A., Lanfranchi, M., Soncini, F., 2016. Nonlinear deformation behaviour of auxetic cellular materials with re-entrant lattice structure. Fatig. Fract. Eng. Mater. Struct. 39, 599–610. https://doi.org/10.1111/ffe.12381.

Chan, N., Evans, K.E., 1998. Indentation resilience of conventional and auxetic foams. J. Cell. Plast. 34, 231–260. https://doi.org/10.1177/0021955X9803400304.

Chan, N., Evans, K.E., 1997. Fabrication methods for auxetic foams. J. Mater. Sci. 32, 5945–5953. https://doi.org/10.1023/A:1018606926094.

Cheng, H.C., Scarpa, F., Hallak Panzera, T., Farrow, I., Peng, H.-X., 2018. Shear stiffness and energy absorption of auxetic open cell foams as sandwich cores. Phys. Status Solidi 256, 1–9. https://doi.org/10.1002/pssb.201800411.

Duncan, O., Allen, T., Birch, A., Foster, L., Hart, J., Alderson, A., 2021. Effect of steam conversion on the cellular structure, Young's modulus and negative Poisson's ratio of closed-cell foam. Smart Mater. Struct. 30, 015031 https://doi.org/10.1088/1361-665X/abc300.

Duncan, O., Allen, T., Foster, L., Senior, T., Alderson, A., 2017. Fabrication, characterisation and modelling of uniform and gradient auxetic foam sheets. Acta Mater. 126, 426–437. https://doi.org/10.1016/j.actamat.2017.01.004.

Duncan, O., Clegg, F., Essa, A., Bell, A.M.T., Foster, L., Allen, T., Alderson, A., 2019. Effects of heat exposure and volumetric compression on Poisson's ratios, Young's moduli, and polymeric composition during thermo-mechanical conversion of auxetic open cell polyurethane foam. Phys. Status Solidi 256. https://doi.org/10.1002/pssb.201800393.

Evans, K.E., Nkansah, M.A., Hutchinson, I.J., Rogers, S.C., 1991. Molecular network design. Nature 353, 124. https://doi.org/10.1038/353124a0.

Gibson, L.J., Ashby, M.F., 1997. Cellular Solids: Structure and Properties. Cambridge University Press, Cambridge, U.K.

Grima, J.N., Attard, D., Gatt, R., Cassar, R.N., 2009. A novel process for the manufacture of auxetic foams and for their re-conversion to conventional form. Adv. Eng. Mater. 11, 533–535. https://doi.org/10.1002/adem.200800388.

ISO, 2011. 13314:2011 - Mechanical Testing of Metals - Ductility Testing - Compression Test for Porous and Cellular Metals. International Organization for Standardization, Geneva, Switzerland.

Jin, S., Korkolis, Y.P., Li, Y., 2019. Shear resistance of an auxetic chiral mechanical metamaterial. Int. J. Solid Struct. 174–175, 28–37. https://doi.org/10.1016/j.ijsolstr.2019.06.005.

Kelkar, P.U., Kim, H.S., Cho, K.H., Kwak, J.Y., Kang, C.Y., Song, H.C., 2020. Cellular auxetic structures for mechanical metamaterials: a review. Sensors 20, 1–26. https://doi.org/10.3390/s20113132.

Kolken, H.M.A., Zadpoor, A.A., 2017. Auxetic mechanical metamaterials. RSC Adv. 7, 5111–5129. https://doi.org/10.1039/C6RA27333E.

Lakes, R.S., 1987. Foam structures with a negative Poisson's ratio. Science 84 235, 1038–1040. https://doi.org/10.1126/science.235.4792.1038.

Li, S., Li, X., Wang, Z., Wu, G., Lu, G., Zhao, L., 2016. Finite element analysis of sandwich panels with stepwise graded aluminum honeycomb cores under blast loading. Composer Part A Appl. Sci. Manuf. 80, 1–12. https://doi.org/10.1016/j.compositesa.2015.09.025.

Li, T., Hu, X., Chen, Y., Wang, L., 2017. Harnessing out-of-plane deformation to design 3D architected lattice metamaterials with tunable Poisson's ratio. Sci. Rep. 7, 8949. https://doi.org/10.1038/s41598-017-09218-w.

Li, Y., Zeng, C., 2016. Room-temperature, near-instantaneous fabrication of auxetic materials with constant Poisson's ratio over large deformation. Adv. Mater. 28, 2822–2826. https://doi.org/10.1002/adma.201505650.

Lira, C., Innocenti, P., Scarpa, F., 2009. Transverse elastic shear of auxetic multi re-entrant honeycombs. Compos. Struct. 90, 314–322. https://doi.org/10.1016/j.compstruct.2009.03.009.

Lurie, S.A., Kalamkarov, A.L., Solyaev, Y.O., Ustenko, A.D., Volkov, A.V., 2018. Continuum micro-dilatation modeling of auxetic metamaterials. Int. J. Solid Struct. 132–133, 188–200. https://doi.org/10.1016/j.ijsolstr.2017.09.022.

Novak, N., Krstulović-Opara, L., Ren, Z., Vesenjak, M., Krstulovic-Opara, L., Ren, Z., Vesenjak, M., 2020. Compression and shear behaviour of graded chiral auxetic structures. Mech. Mater. 148 https://doi.org/10.1016/j.mechmat.2020.103524.

Phillips, N., Hassan, G.M., Dyskin, A., Macnish, C., Pasternak, E., 2018. Digital image correlation to analyse nonlinear elastic behavior of materials. In: Proc. - Int. Conf. Image Process. ICIP 2017-Septe. https://doi.org/10.1109/ICIP.2017.8297107.

Shepherd, T., Winwood, K., Venkatraman, P., Alderson, A., Allen, T., 2020. Validation of a finite element modeling process for auxetic structures under impact. Phys. Status Solidi Basic Res. 257, 1–14. https://doi.org/10.1002/pssb.201900197.

Stelman, H.J., 2018. Chapter 6 the t-test and basic inference principles. In: Experimental Design and Analysis. CMU Statistics, pp. 141–170.

Timoshenko, S.P., Goodier, J.N., 1970. Theory of Elasticity, third ed. McGraw-Hill, USA, New York.

Zhu, H.X., Knott, J.F., Mills, N.J., 1997. Analysis of the elastic properties of open-cell foams with tetrakaidecahedral cells. J. Mech. Phys. Solid. 45.